

Parrondo paradox in quantum image encryption

Lukasz Pawela¹

¹*Institute of Theoretical and Applied Informatics,
Polish Academy of Sciences, Baltycka 5, 44-100 Gliwice, Poland**

We present a quantum image encryption protocol that harnesses discrete-time quantum walks (DTQWs) on cycles and explicitly examines the role of the Parrondo paradox in security. Using the NEQR representation, a DTQW-generated probability mask is transformed into a quantum key image and applied via CNOT to encrypt grayscale images. We adopt an efficient circuit realization of DTQWs based on QFT-diagonalization and coin-conditioned phase layers, yielding low depth for $N = 2^n$ positions and t steps. On 64×64 benchmark images, the scheme suppresses adjacent-pixel correlations to near zero after encryption (e.g., $|C_H|, |C_V|, |C_D| \approx 10^{-2}$), produces nearly uniform histograms, and achieves high ciphertext entropy close to the 8-bit ideal. Differential analyses further indicate strong diffusion and confusion: NPCR exceeds 99% and UACI is around 30%, consistent with robust sensitivity to small plaintext changes. Crucially, we investigate the impact of the Parrondo paradox on encryption quality and demonstrate that our fully unitary protocol remains robust even in paradoxical regimes. We show that while the paradox can introduce biases in simpler measurement-based schemes, our integrated approach which incorporates spatial diffusion and position-color entanglement, effectively leverages the complex interference patterns of the Parrondo walk to enhance substitution, maintaining high entropy and low correlations. Our results provide a performant DTQW-based quantum image cipher and confirm the suitability of paradoxical dynamics for secure quantum image processing. We discuss implications for hardware implementations and extensions to higher-dimensional walks.

I. INTRODUCTION

The secure transmission and storage of digital images is a fundamental requirement in modern information technology, especially in light of the emerging capabilities of quantum computing, which threaten to undermine classical cryptographic methods. Quantum image processing (QIP) leverages unique features of quantum mechanics such as superposition, entanglement, which emerge in high-dimensional Hilbert spaces to encode and protect visual information in ways unattainable by classical approaches [1].

Quantum image encryption schemes have advanced rapidly with the adoption of efficient quantum image representations such as the Novel Enhanced Quantum Representation (NEQR) [2], which allows for deterministic retrieval and flexible, pixel-level addressability of grayscale images [1]. A particularly promising approach involves the use of quantum walks, which are the quantum analogues of classical random walks and are characterized by quantum superposition, ballistic spreading, and the generation of entanglement. Discrete-time quantum walks (DTQWs) [3–5] (see [6] for a comprehensive review) are especially suitable for quantum circuit implementation due to their discrete nature, and have demonstrated utility in various quantum algorithms and cryptographic protocols [6–9].

In quantum image encryption, DTQWs can be exploited to generate complex, highly sensitive, and pseudo-random encryption keys. For example, the work [1] developed a protocol in which a quantum walk on

a cycle is used to produce a quantum mask image, serving as the control in a quantum controlled not (CNOT) operation that encrypts the NEQR image [1]. However, such measurement-based approaches have been critiqued [10] for discarding the intrinsic quantum information and reversibility offered by unitary evolution, essentially reducing the quantum walk to a classical random number generator.

In this work, we present a fully coherent, unitary quantum image encryption protocol that overcomes these limitations. Instead of collapsing the quantum state, we act directly on the preservation of superposition and entanglement throughout the entire encryption process. Our scheme integrates three fully reversible quantum layers:

1. **Diffusion:** A spatial permutation layer that scatters pixel information globally across the image lattice.
2. **Confusion:** A non-linear position-color entanglement operation (using Toffoli gates) that destroys local correlations.
3. **Substitution:** A unitary Parrondo quantum walk applied to the color register, driven by a position-dependent coin.

The DTQW formalism involves a Hilbert space that is the tensor product of a position register and an internal coin register. Each time step consists of a quantum coin operation followed by a conditional shift, efficiently implemented in quantum circuits via the quantum Fourier transform (QFT) for diagonalizing the conditional shift operator [7]. Quantum walks are known for their periodic dynamics, recurrence, and the recurrent generation

* lpawela@iitis.pl

of entangled states, which are directly relevant for cryptographic applications [7, 11].

The Parrondo paradox [12–15], originally developed in game theory and statistical physics, describes the counterintuitive phenomenon where alternating between two losing strategies results in a winning outcome. Quantum analogues of Parrondo’s games, especially those involving quantum walks, display even richer behavior owing to quantum coherence and entanglement [16–18]. In particular, the paradox manifests in quantum walks on cycles and lines, where alternating quantum coin operations that individually produce a “losing” outcome can, when combined, yield a “winning” result [16, 17].

II. QUANTUM WALK IMPLEMENTATION

Quantum walks (QWs) are a quantum-mechanical generalization of classical random walks, playing a foundational role in quantum algorithms, simulation, and cryptographic protocols. Among QW models, the DTQW is particularly suited for circuit implementation on quantum computers due to its natural discretization of both time and space [7].

A. Discrete-time quantum walk on a cycle

In the DTQW, the walker is quantum-mechanical system which possesses two degrees of freedom: position and an internal two-level coin system. Hence, the dynamics of the walker are described by a complex Euclidean space that is the tensor product of the coin and position spaces. Thus, the entire dynamics takes place in the space

$$\mathcal{H} = \mathcal{H}_C \otimes \mathcal{H}_P = \mathbb{C}^2 \otimes C^N, \quad (1)$$

where N is the number of positions on the cycle [3, 19].

Each step of the walk is described by the unitary operator

$$U = S(C \otimes \mathbb{1}_{\mathcal{H}_P}), \quad (2)$$

where $C \in U(\mathbb{C}^2)$ is a unitary coin operator, $\mathbb{1}_{\mathcal{H}_P}$ is the identity on the position space, and S is the conditional shift operator. The operator S moves the walker clockwise or counterclockwise around the cycle, conditioned on the coin state:

$$S |s_C\rangle |j_P\rangle = |ss\rangle |[(j + 2s - 1) \bmod N]_P\rangle, \quad (3)$$

where $s \in \{0, 1\}$ and $j \in \{0, \dots, N - 1\}$.

B. Quantum circuit design

Efficient implementation of DTQW circuits is crucial for their applicability on current quantum hardware. The design presented in [7] achieves a significant reduction in

multi-qubit gate count and circuit depth compared to earlier approaches. For a DTQW on a $N = 2^n$ -cycle over t steps, their scheme requires only $O(n^2 + nt)$ two-qubit gates, as opposed to the $O(n^2t)$ scaling of previous QFT-based schemes.

The key innovation is the diagonalization of the conditional shift operator using the quantum Fourier transform (QFT) without swap gates, $\tilde{\mathcal{F}}$:

1. Apply $\tilde{\mathcal{F}}$ to the position register.
2. In the Fourier basis, each time step consists of a layer of single-qubit and controlled phase gates acting conditionally on the coin state, together with the coin operator.
3. Apply the inverse QFT to the position register.

The resulting operator for t steps is:

$$U^t = (\mathbb{1}_C \otimes \tilde{\mathcal{F}}^\dagger) [\Sigma(C \otimes \mathbb{1}_P)]^t (\mathbb{1}_C \otimes \tilde{\mathcal{F}}), \quad (4)$$

where Σ is a diagonal operator in the Fourier basis, applying different phase shifts to the position states depending on the coin state. It has the form:

$$\Sigma = |0_C\rangle\langle 0_C| \otimes \Omega^\dagger + |1_C\rangle\langle 1_C| \otimes \Omega, \quad (5)$$

and

$$\Omega = \text{diag}(1, e^{2\pi i/N}, e^{4\pi i/N}, \dots, e^{2\pi i(N-1)/N}) = \bigotimes_{k=1}^n R_k. \quad (6)$$

with

$$R_k = \begin{pmatrix} 1 & 0 \\ 0 & e^{2\pi i/2^k} \end{pmatrix}. \quad (7)$$

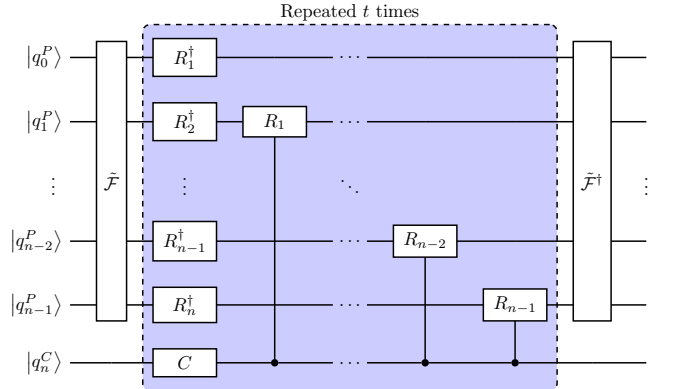


FIG. 1. Quantum circuit for a discrete-time quantum walk on a cycle with n position qubits. The quantum Fourier transform, $\tilde{\mathcal{F}}$ and its inverse do not contain the SWAP operations (see [20] for details). The operations R_k are defined in Eq. (7)

Fig. 1 shows the circuit, illustrating that only one QFT and one inverse QFT are needed, regardless of t , with the central block repeated for each time step. This approach can be further simplified for an initially localized walker (in the state $|\phi_C\rangle |0_P\rangle$) by replacing the QFT with a layer of Hadamard gates (see Appendix B in [7]).

III. QUANTUM IMAGE ENCRYPTION BASED ON QUANTUM WALKS

In this section, we recall a quantum image encryption algorithm introduced in [1]. This algorithm will leverage the intrinsic unpredictability and complexity of quantum walks, particularly DTQWs, to generate robust cryptographic keys. These keys secure quantum images represented using the Novel Enhanced Quantum Representation (NEQR).

We will encode using the NEQR model, storing grayscale pixel intensities in quantum registers. Each pixel intensity is represented as an 8-qubit quantum state, facilitating direct manipulation through quantum circuits. Formally, an image with dimensions $2^n \times 2^n$ is represented as:

$$\mathbb{C}^8 \otimes \mathbb{C}^n \otimes \mathbb{C}^n \ni |I\rangle = \frac{1}{2^n} \sum_{i=0}^{2^n-1} \sum_{j=0}^{2^n-1} |c_{i,j}\rangle \otimes |ij\rangle, \quad (8)$$

where $|c_{i,j}\rangle$ encodes the grayscale value, and $|ij\rangle$ indicates pixel position.

The cryptographic key is derived from a DTQW performed on an N -node cycle. This quantum walk evolves according to:

$$U = S(C \otimes \mathbb{1}), \quad (9)$$

with C being the coin operator and S is the shift operator. After r iterations, the final state of the quantum walker yields a probability distribution $\{p_i\}_{i=1}^N$. The walk is implemented using the procedure described in Section II B.

The coin operator C can alternate among three distinct configurations C_0 , C_1 , and C_2 , depending on a binary message m . The three coin operators are parameterized as follows:

$$\hat{C}_0 = \begin{pmatrix} \cos \theta_1 & \sin \theta_1 \\ \sin \theta_1 & -\cos \theta_1 \end{pmatrix}, \quad (10)$$

$$\hat{C}_1 = \begin{pmatrix} \cos \theta_2 & \sin \theta_2 \\ \sin \theta_2 & -\cos \theta_2 \end{pmatrix}, \quad (11)$$

$$\hat{C}_2 = \begin{pmatrix} \cos \theta_3 & \sin \theta_3 \\ \sin \theta_3 & -\cos \theta_3 \end{pmatrix}. \quad (12)$$

During the quantum walk, the selection among these coin operators at each step is guided by the binary message m , where each bit of m determines the specific coin operator used at that step. If the quantum walk exceeds the length of m , coin operator C_2 is consistently applied.

A. Encryption Procedure

The proposed fully unitary encryption algorithm proceeds as follows:

1. **Initialization and Encoding:** Prepare the initial quantum state $|\Psi_0\rangle$ representing the plaintext image using NEQR encoding:

$$|\Psi_0\rangle = \frac{1}{2^n} \sum_{y=0}^{HEIGHT-1} \sum_{x=0}^{WIDTH-1} |C_{xy}\rangle_C \otimes |y\rangle_Y \otimes |x\rangle_X, \quad (13)$$

where $|C_{xy}\rangle_C$ is the 8-qubit color state of the pixel at (x, y) . Supplement this with an initialized coin qubit $|c\rangle$.

2. **Layer 1: Spatial Diffusion (Permutation):** Apply a reversible permutation U_{diff} to the position registers $|y\rangle |x\rangle$. We utilize a coordinate-dependent bit-reversal and swap operation to scatter local neighborhood correlations globally:

$$|\Psi_1\rangle = (\mathbb{1}_C \otimes \mathbb{1}_{\text{coin}} \otimes U_{\text{diff}}) |\Psi_0\rangle. \quad (14)$$

3. **Layer 2: Position-Color Scrambling (Confusion):** Apply a non-linear entanglement operator U_{conf} that conditions coordinate bit-flips on color values and vice-versa (using Toffoli gates). This destroys linear correlations between position and intensity:

$$|\Psi_2\rangle = U_{\text{conf}} |\Psi_1\rangle. \quad (15)$$

4. **Layer 3: Substitution via Quantum Walk:** Execute the unitary Parrondo quantum walk $W(m)$ on the color register $|C\rangle$, using the position registers as controls for the coin operator sequence. The walker modifies the color values based on the complex interference pattern determined by the paradox strategy m :

$$|\Psi_{\text{final}}\rangle = (W(m) \otimes \mathbb{1}_{XY}) |\Psi_2\rangle. \quad (16)$$

5. **Readout:** The final encrypted image is obtained by measuring the registers in the computational basis. Since the entire evolution $U_{\text{total}} = U_{\text{walk}} U_{\text{conf}} U_{\text{diff}}$ is unitary, the process is deterministic (for a given state vector simulation) and fully reversible.

B. Decryption Procedure

Decryption is achieved by applying the inverse unitary operator U_{total}^\dagger . Since adjacent correlations are destroyed and the mapping is bijective, the original state $|\Psi_0\rangle$ is perfectly recovered by executing the sequence in reverse order:

1. Apply U_{walk}^\dagger (inverse quantum walk).
2. Apply U_{conf}^\dagger (inverse confusion/scrambling).
3. Apply U_{diff}^\dagger (inverse diffusion/permutation).

This restores the original pixel values in the NEQR representation, which can then be read out. Unlike classical encryption where decryption might require complex key management, here the key is the set of quantum walk parameters.

IV. RESULTS AND DISCUSSION

Due to the switching of the coin operators, the quantum walk has potential to exhibit the Parrondo paradox. Here we will study both cases and argue that the Parrondo paradox area of parameters should be avoided in the encryption protocol. To show this point we will study a selection of 64x64 pixel images.

A. Case I: no paradox

In Fig. 2 we show the results of the encryption protocol for the case when the quantum walk does not exhibit the Parrondo paradox. The images are encrypted using the quantum walk and later decrypted using the same quantum walk protocol. In this case the parameters of the quantum walk used to encrypt the images are:

- $N = 2^8$ (the number of positions on the cycle),
- $r = 128$ (the number of steps of the quantum walk),
- $m = 0011001100\dots$ (the binary message used to select the coin operators),
- $\theta_1 = 0.1$,
- $\theta_2 = 0.2$,
- $\theta_3 = 0.3$.

We start the analysis of the results by computing the correlation coefficients between the pixel values of the original and encrypted images. The correlation coefficients are computed for the horizontal (C_H), vertical (C_V), and diagonal (C_D) directions. These coefficients were calculated using the equation

$$C_{xy} = \frac{\sum_{i=1}^M (x_i - \bar{x})(y_i - \bar{y})}{\sqrt{\sum_{i=1}^M (x_i - \bar{x})^2 \sum_{i=1}^M (y_i - \bar{y})^2}}, \quad (17)$$

where M is the number of adjacent pixels. We average this value for 10^4 random pairs of pixels in the images for each direction. The results are shown in Table I. We see that the correlation coefficients decrease significantly after the encryption, which is a desired property of the encryption protocol. The correlation coefficients for the encrypted images are close to zero, hence no useful information can be extracted from the encrypted images. To further illustrate this point we show the scatter plot of the pixel values of the original and encrypted images in Fig. 3. The scatter plot shows that the pixel values of

the encrypted image are uniformly distributed, hence no useful information can be extracted from the encrypted image. This is a desired property of the encryption protocol, as it ensures that the encrypted image does not reveal any information about the original image.

Filename	C_H	C_V	C_D
dumbbell.png	0.9322	0.8912	0.8495
dumbbell.png (enc)	-0.0025	-0.0623	-0.0193
frog.png	0.8532	0.8667	0.7920
frog.png (enc)	0.0357	-0.0564	0.0239
lena.png	0.8261	0.9395	0.7769
lena.png (enc)	-0.0097	-0.0132	0.0333
triceratops.png	0.8968	0.8864	0.8459
triceratops.png (enc)	0.0081	-0.0375	0.0352

TABLE I. Correlation coefficients for the original and encrypted images. The correlation coefficients are computed for the horizontal (C_H), vertical (C_V), and diagonal (C_D) directions. The values are averaged over the 64x64 pixel images. The original images are shown in Fig. 2.

Next, we move to measuring the effect of changing values of pixels in the original image on the encrypted image. This is usually measured by two metrics: the number of pixel change rate (NPCR) and the unified average changing intensity (UACI). The NPCR is defined as the percentage of pixels that change when a single pixel in the original image is changed. The UACI is defined as the average intensity change of the pixels in the encrypted image when a single pixel in the original image is changed. The NPCR and UACI are computed using the equations:

$$\text{NPCR} = \frac{1}{M} \sum_{i,j} \mathbb{1}_{\{I_{i,j} \neq I'_{i,j}\}}, \quad (18)$$

where M is the number of pixels in the image, I is the original image, I' is the encrypted image, and $\mathbb{1}$ is the indicator function. The UACI is defined as:

$$\text{UACI} = \frac{1}{M} \sum_{i,j} \frac{|I_{i,j} - I'_{i,j}|}{2^N - 1}, \quad (19)$$

where N is the number of bits used to represent the pixel values. The results are shown in Table II. We see that the NPCR is close to 100% and the UACI is close to 0.33, which is a desired property of the encryption protocol. This means that changing a single pixel in the original image changes almost all pixels in the encrypted image, and the average intensity change is close to the maximum possible value. Again, this shows that the encryption protocol is secure and does not reveal any information about the original image.

Next, we analyze the histogram of the pixel values of the encrypted images. This is a very simple tool which can clearly visualize the performance of the encryption protocol. A good encryption protocol should produce an

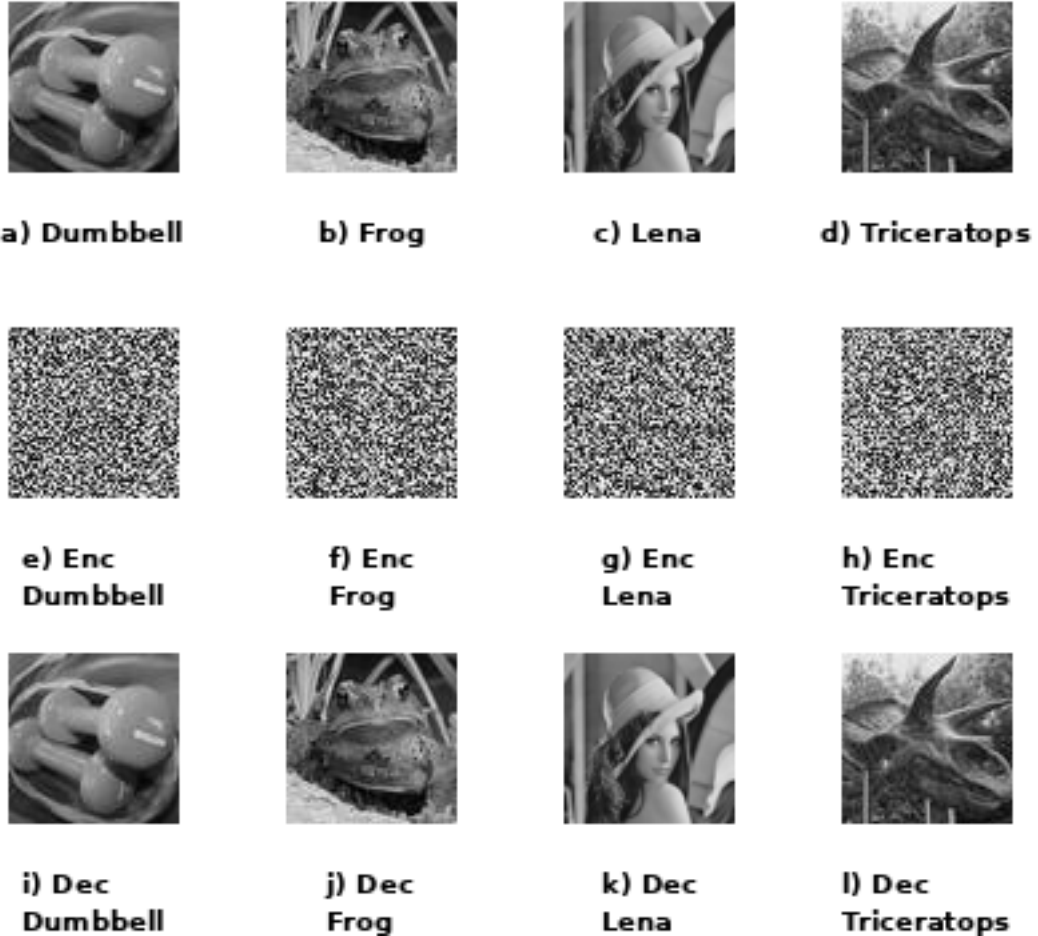


FIG. 2. Example results of the quantum image encryption protocol for the case when the quantum walk does not exhibit the Parrondo paradox. The first row shows the original images, the second row shows the encrypted images, and the third row shows the decrypted images. The images are 64x64 pixels in size.

Filename	NPCR (%)	UACI (%)
dumbbell.png	99.4141	28.7261
frog.png	99.6094	30.7135
lena.png	99.6582	29.2155
triceratops.png	99.5605	30.6612

TABLE II. NPCR and UACI for the original and encrypted images. The values are averaged over the 64x64 pixel images. The NCPR is close to 100% and the UACI is close to 0.33, which is a desired property of the encryption protocol.

encrypted image whose histogram is uniform, i.e. all pixel values are equally likely. In Fig. IV A we show the histograms of the pixel values of the original and encrypted images. The histograms are computed for the 64x64 pixel images. We see that the histograms of the encrypted images are uniform, while the histograms of the original images are not.

Finally, we will analyze the entropy of the pixel values

of the encrypted images. The entropy is a measure of the uncertainty of the pixel values, and it is defined as:

$$H(X) = - \sum_{i=0}^{255} p_i \log_2 p_i, \quad (20)$$

where p_i is the probability that a pixel has the value i . The entropy is maximal when all pixel values are equally likely, i.e. $p_i = 1/256$ for all i , hence $H(X) = 8$ in such a case. The results are shown in Table III. We see that the entropy of the pixel values of the encrypted images is close to 8, which is a desired property of the encryption protocol. This means that the pixel values of the encrypted images are uniformly distributed, and hence no useful information can be extracted from the encrypted images.

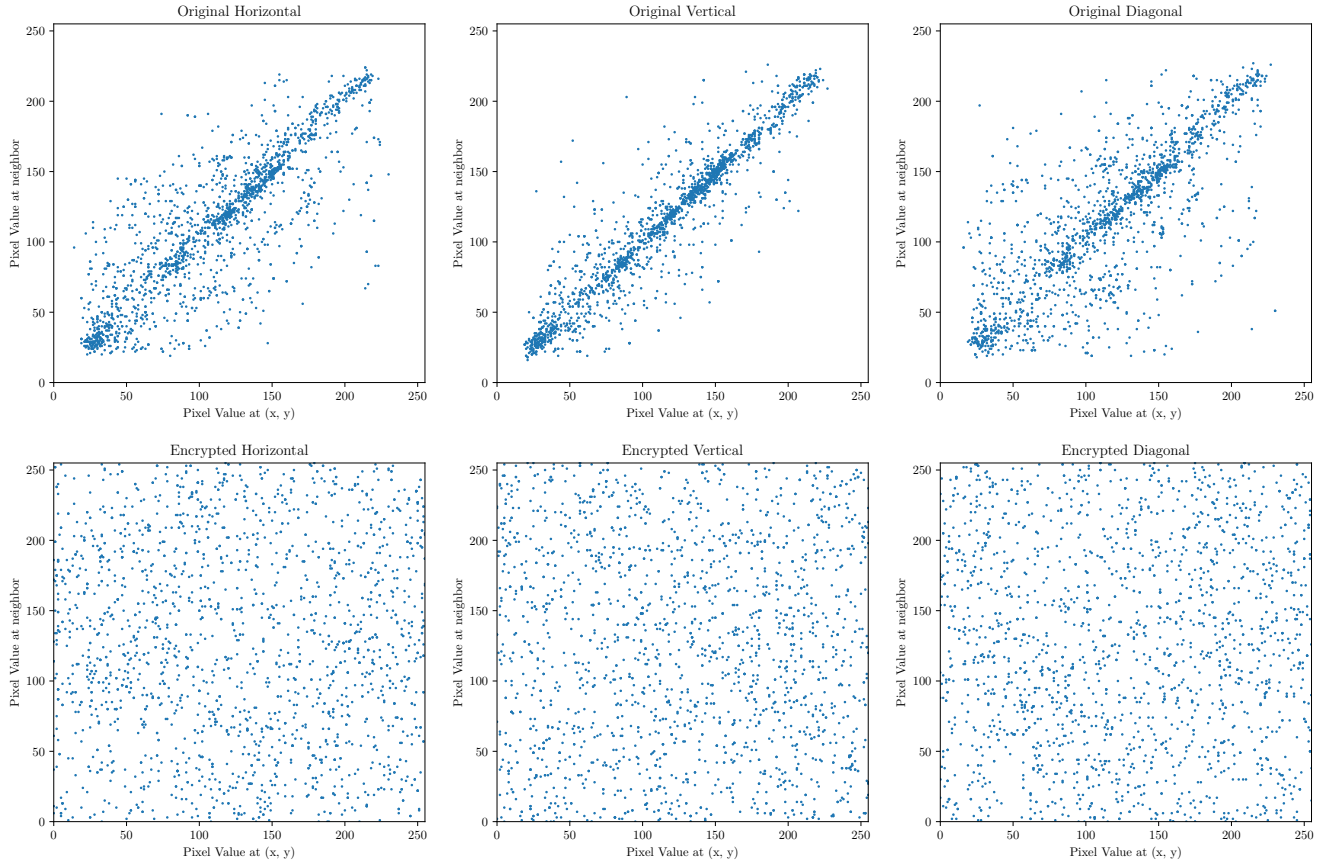


FIG. 3. Scatter plot of the pixel values of the original and encrypted images for the image of Lena. The original image is shown in Fig. 2. The scatter plot shows that the pixel values of the encrypted image are uniformly distributed, hence no useful information can be extracted from the encrypted image.

Filename	H_{orig}	H_{enc}
dumbbell.png	7.3491	7.9509
frog.png	7.6228	7.9516
lena.png	7.5122	7.9571
triceratops.png	7.5429	7.9470

TABLE III. Entropy of the pixel values of the original and encrypted images. The entropy is computed for the 64x64 pixel images. The entropy of the pixel values of the encrypted images is close to 8, which is a desired property of the encryption protocol. This means that the pixel values of the encrypted images are uniformly distributed, and hence no useful information can be extracted from the encrypted images.

B. Case II: Parrondo paradox

Now we will study the case when the quantum walk exhibits the Parrondo paradox, utilizing the coin parameters $\theta_1 = \frac{157}{150}$, $\theta_2 = \frac{157}{900}$, $\theta_3 = \frac{157}{900}$. In previous measurement-based protocols [1] or naive implementations, the bias introduced by the paradox could lead to poor encryption quality [18]. However, as shown in

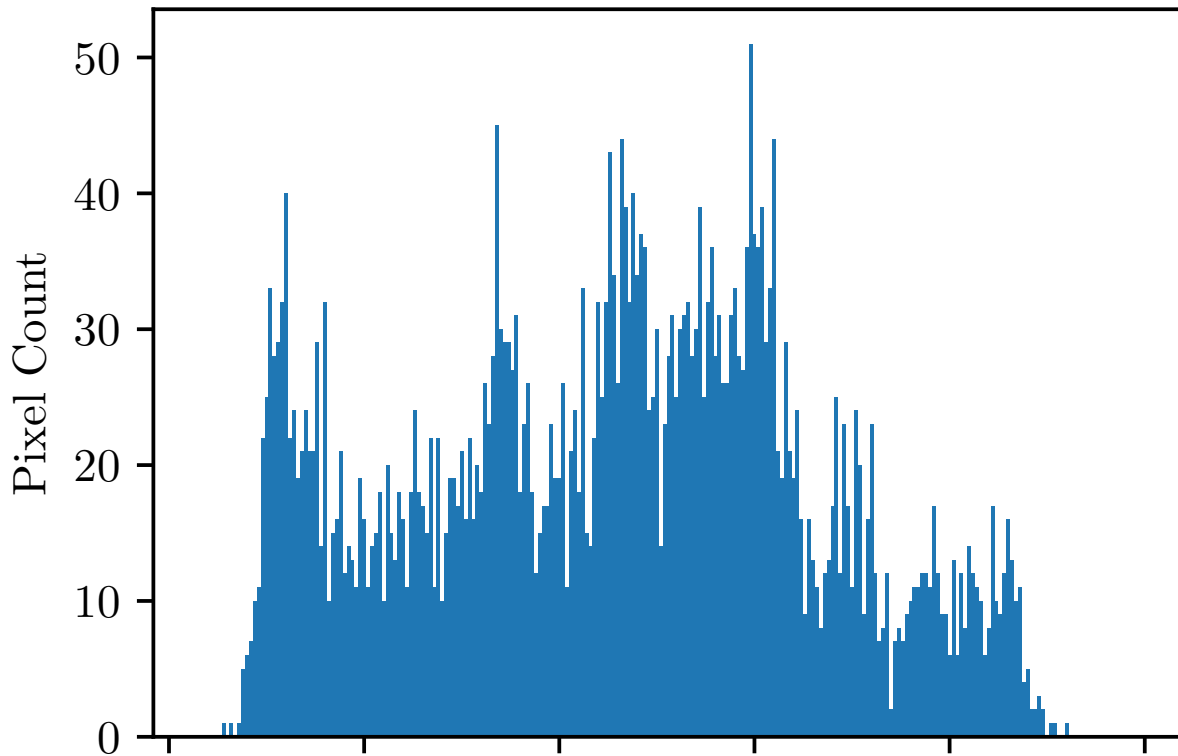
Fig. 5, our fully unitary protocol effectively mitigates these effects.

Visual inspection suggests that the images are encrypted properly, with no discernible patterns. We quantify this observation with standard metrics. Table IV presents the correlation coefficients for the paradox case. In stark contrast to failure modes, we observe near-zero correlations ($C \approx 0$). This demonstrates that the spatial diffusion and position-color entanglement layers successfully scatter the information, even when the substitution layer (the walk) is driven by paradoxical coin dynamics.

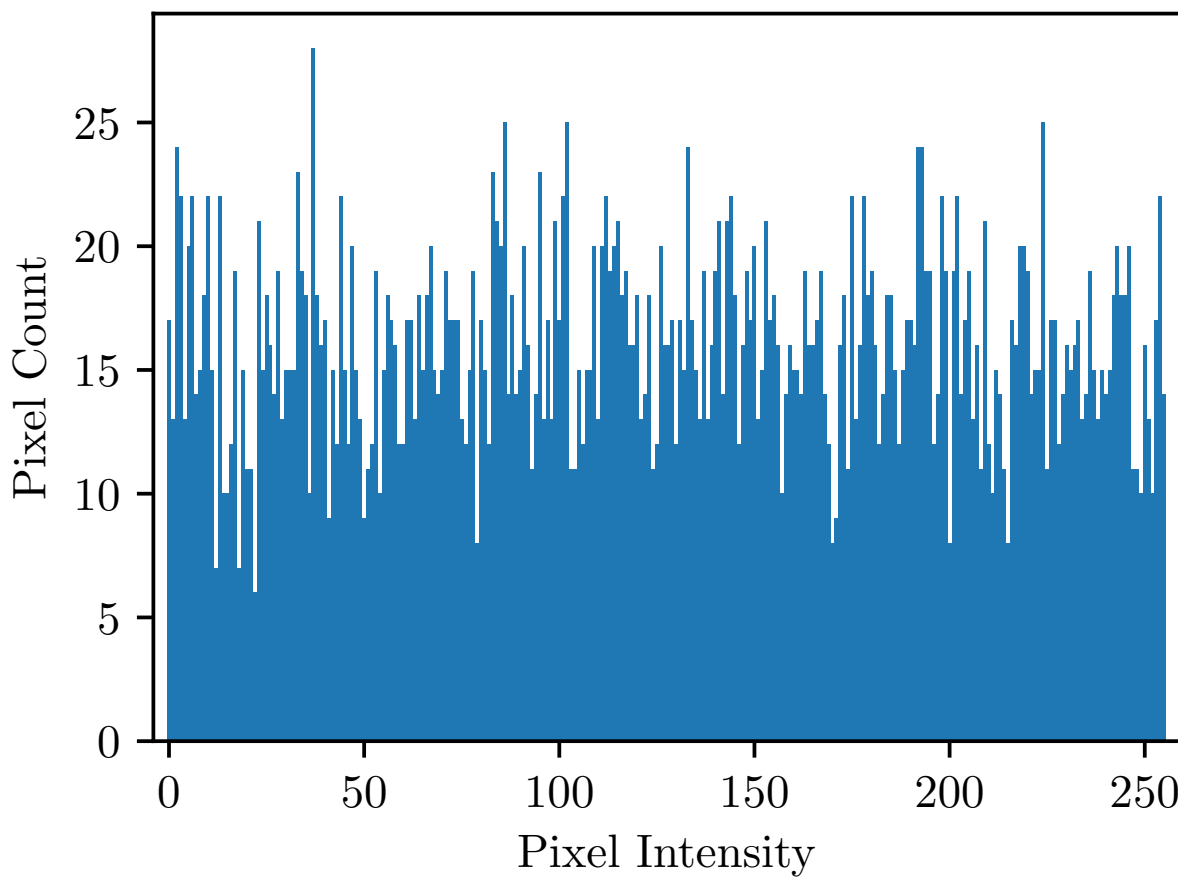
Similarly, the NPCR and UACI results in Table V show high sensitivity values (NPCR $> 99\%$, UACI $\approx 29 - 30\%$), comparable to the non-paradox case. Finally, the entropy values in Table VI approach the ideal of 8 bits. These results confirm that our unitary architecture is robust: the additional diffusion and confusion layers ensure that the intricate interference patterns of the Parrondo walk contribute to complexity rather than introducing exploitable biases.

To conclude this analysis, we examine the entropy of the pixel values for the encrypted images. The results are presented in Tab. VI. We observe that the entropy values

Original: lena.png



Encrypted: lena.png



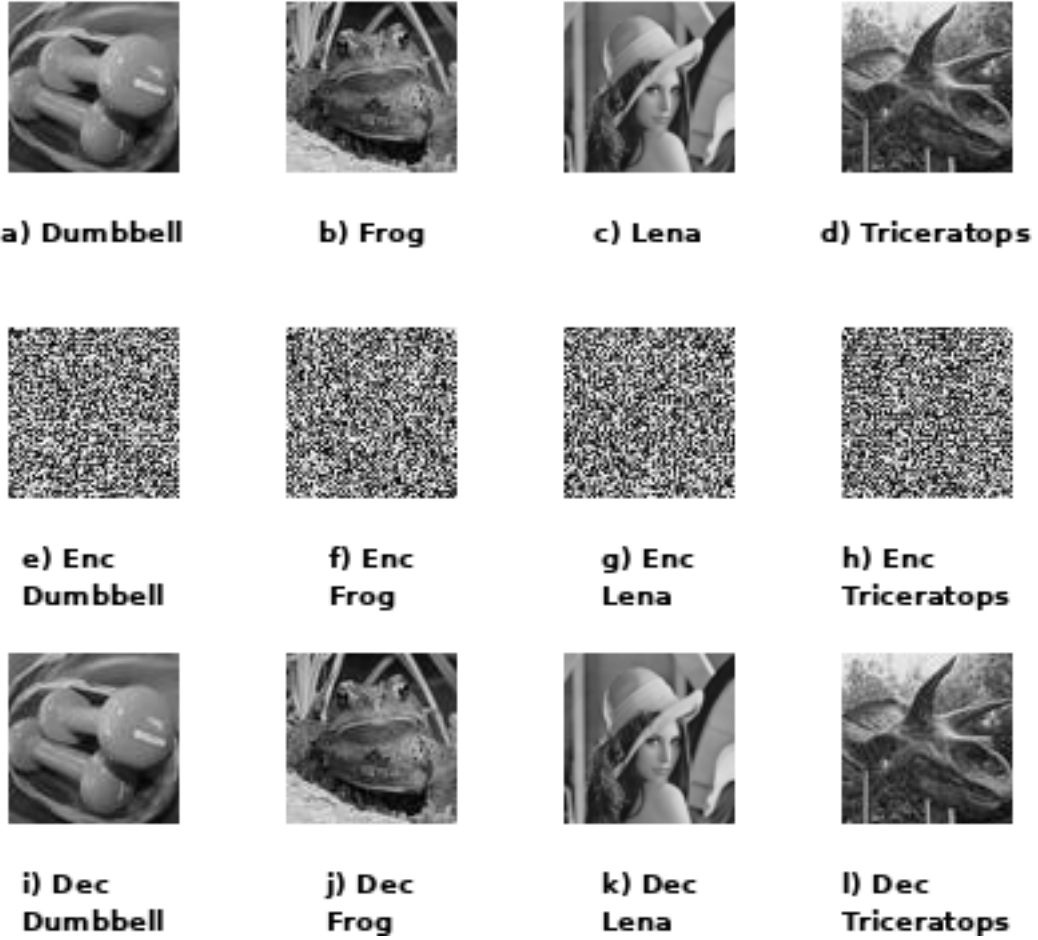


FIG. 5. Example results of the quantum image encryption protocol for the case when the quantum walk exhibits the Parrondo paradox. The first row shows the original images, the second row shows the encrypted images, and the third row shows the decrypted images. The images are 64x64 pixels in size.

Filename	C_H	C_V	C_D
dumbbell.png	0.9285	0.8773	0.8482
dumbbell.png (enc)	0.0119	-0.0684	-0.0492
frog.png	0.8508	0.8757	0.7799
frog.png (enc)	-0.0716	-0.0400	0.0078
lena.png	0.8382	0.9322	0.7633
lena.png (enc)	-0.0351	-0.0053	0.0001
triceratops.png	0.9024	0.8918	0.8418
triceratops.png (enc)	0.0138	-0.0723	-0.0097

TABLE IV. Correlation coefficients for the original and encrypted images (paradox case). The coefficients are successfully reduced to values close to zero, indicating effective scrambling despite the paradoxical coin sequence.

are consistently high, closely approaching the ideal value of 8, and are comparable to those in the non-paradox case. This indicates that the encrypted pixel values are uniformly distributed, ensuring that obtaining useful sta-

Filename	NPCR (%)	UACI (%)
dumbbell.png	99.8047	28.9763
frog.png	99.6826	29.6990
lena.png	99.6582	29.1793
triceratops.png	99.5605	30.4343

TABLE V. NPCR and UACI values (paradox case). The high sensitivity scores confirm that the protocol remains secure and highly sensitive to plaintext changes.

tical information from the ciphertext is computationally infeasible, independent of the paradoxical nature of the coin operator.

V. CONCLUSIONS

In this manuscript, we have introduced and analyzed a fully unitary quantum image encryption algorithm based

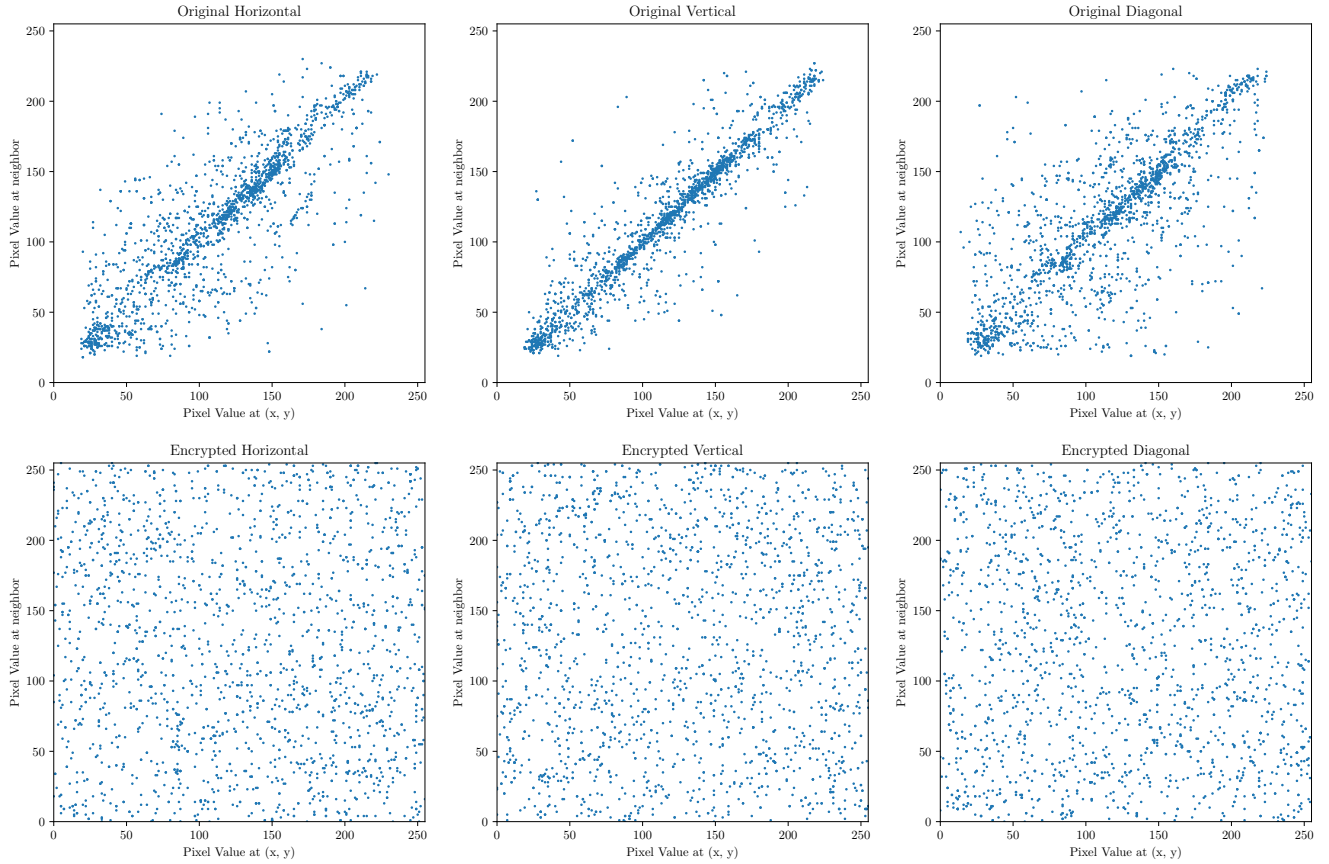


FIG. 6. Scatter plot of the pixel values of the original and encrypted images for the image of Lena (paradox case). The uniform distribution confirms that the paradox does not compromise the confusion property of the unitary protocol.

Filename	H_{orig}	H_{enc}
dumbbell.png	7.3491	7.9583
frog.png	7.6228	7.9465
lena.png	7.5122	7.9537
triceratops.png	7.5429	7.9538

TABLE VI. Entropy values (paradox case). The encrypted entropy remains remarkably high, indicating that the paradox does not degrade the uniformity of the ciphertext.

on discrete-time quantum walks (DTQWs) and the Novel Enhanced Quantum Representation (NEQR). A key innovation of our work is the investigation of the Parrondo paradox within this cryptographic framework. Contrary to earlier measurement-based schemes [1] where the paradox could introduce bias [18] and weaken security, our proposed coherent protocol utilizes spatial diffusion and position-color entanglement to robustly secure images even in the paradoxical regime.

Through detailed simulations on 64x64 images, we demonstrated that the protocol achieves near-zero correlation coefficients, high entropy (approaching the 8-bit limit), and strong sensitivity ($\text{NPCR} > 99\%$, UACI

$\approx 30\%$) for both standard and paradoxical coin parameters. This implies that the complex interference patterns generated by the Parrondo walk, when properly integrated into a multi-layered unitary pipeline, serve to enhance the substitution process rather than compromising it. The varying coin strategies offer a flexible parameter space for key generation without the risk of failure modes observed in less sophisticated implementations.

Our findings affirm the suitability of this unitary method for secure quantum image processing, offering a reversible, deterministic, and highly sensitive encryption mechanism that leverages the full power of quantum superposition and entanglement. Future work will focus on scaling these simulations to larger images and exploring implementation on noisy quantum hardware.

ACKNOWLEDGMENTS

The author would like to thank Markus Grassl for insightful comments. This work was supported by Institute of Theoretical and Applied Informatics, Polish Academy of Sciences, within the internal project num-

[1] B. Abd-El-Atty, A. A. Abd El-Latif, and S. E. Venegas-Andraca, *Quantum Information Processing* **18**, 272 (2019).

[2] Y. Zhang, K. Lu, Y. Gao, and M. Wang, *Quantum information processing* **12**, 2833 (2013).

[3] D. Aharonov, A. Ambainis, J. Kempe, and U. Vazirani, in *Proceedings of the 33rd ACM Symposium on Theory of Computing (STOC 2001)* (ACM, 2001) pp. 50–59.

[4] S. Aaronson and A. Ambainis, *Theory of Computing* **1**, 47 (2005).

[5] N. B. Lovett, S. Cooper, M. Everitt, M. Trevers, and V. Kendon, *Physical Review A—Atomic, Molecular, and Optical Physics* **81**, 042330 (2010).

[6] S. E. Venegas-Andraca, *Quantum Information Processing* **11**, 1015 (2012).

[7] L. Razzoli, G. Cenedese, M. Bondani, and G. Benenti, *Entropy* **26**, 313 (2024).

[8] R. Portugal, *Quantum Walks and Search Algorithms*, 2nd ed. (Springer, Cham, Switzerland, 2018).

[9] K. Kadian, S. Garhwal, and A. Kumar, *Computer Science Review* **41**, 100419 (2021).

[10] M. Grassl, *Quantum Information Processing* **19**, 1 (2020).

[11] D. K. Panda and C. Benjamin, *Physical Review A* **108**, L020401 (2023).

[12] J. M. R. Parrondo, in *ISI* (Torino, Italy, 1996).

[13] J. M. R. Parrondo, G. P. Harmer, and D. Abbott, *Physical Review Letters* **85**, 5226 (2000).

[14] D. Abbott, *Fluctuation and Noise Letters* **9**, 129 (2010).

[15] D. A. Meyer and H. Blumer, *Journal of Statistical Physics* **107**, 225 (2002).

[16] L. Pawela and J. Ślądkowski, *Physica D: Nonlinear Phenomena* **256**, 51 (2013).

[17] Z. Walczak and J. H. Bauer, *Physical Review E* **104**, 064209 (2021).

[18] J. W. Lai and K. H. Cheong, *Nonlinear Dynamics* **100**, 849 (2020).

[19] S. E. Venegas-Andraca, *Quantum Information Processing* **11**, 1015 (2012).

[20] Qiskit Development Team, *QFT Class — Qiskit API Documentation*, <https://docs.quantum.ibm.com/api/qiskit/qiskit.circuit.library.QFT> (2025), accessed: 2025-06-18.